H2020 FETOPEN: OPTO SILICON 964191

This project has received funding from the European Union's Horizon 2020 research and innovation program under grant agreement No 964191.

D1.3 Improved surface passivation, contact formation and electrical characterization [M24]

Type of this document	Report
Dissemination level	Public
Date	April 15, 2023
WP	1
Authors	Willem-Jan Berghuis, Marvin van Tilburg, Wouter Peeters, Victor van Lange, Bart Macco, Marcel Verheijen, Erik Bakkers, Erwin Kessels, Jos Haverkort, Isabelle Bollier, Heinz Schmid
Status	Approved by the whole consortium

This deliverable reflects only the author's view and the Commission is not responsible for any use that may be made of the information it contains.

DESCRIPTION OF DELIVERABLE

Surface passivation, contact formation and electrical characterization of HexSiGe nanowires are reported. The deliverable is structured in two parts. The first part lead by TU/e covers all results on surface passivation using dielectric shells. The second part lead by IBM reports on electrical contact processes and doping for n-type and p-type regions.

1. INTRODUCTION: SURFACE PASSIVATION

The continuous pursuit of technological progress has raised an increasing interest in optical communication (e.g. optical interconnects[1–4]) and light processing devices (e.g. lab-on-a-chip[5]), which both require efficient light sources and detectors compatible with current silicon electronics. Although the natural crystal structure of Ge (diamond cubic) does not exhibit a direct bandgap, it was predicted[6] and recently shown experimentally by Fadaly *et al.*[7] that the hexagonal crystal structure shows efficient direct bandgap emission. The hex-Ge was realized using GaAs/Ge core/shell nanowires (NWs). Besides this, Fadaly *et al.*[7] demonstrated that the bandgap is tunable from 0.3 eV to 0.7 eV by alloying the hex-Ge with 0 to 35 percent Si[7]. This makes hex-SiGe alloys a very promising candidate as silicon-compatible light emitters and absorbers, such as LEDs, lasers and photodetectors compatible with Si-photonics circuitry.

Optical characterization of the hexagonal GaAs/SiGe core/shell nanowires by Fadaly *et al.*[7] revealed that the photoluminescence (PL) efficiency is significantly lower at room temperature (~300 K) than at a few Kelvin (~6 K). The latter indicates most likely the presence of non-radiative recombination pathways. For nanostructures like nanowires, surface-to-volume ratios are relatively large and surface defects can consequently play a much more pronounced role than in a planar structure. Surface recombination via defects at the surface of the hex-(Si)Ge crystals is therefore one of the primary suspects.

In this study, it is investigated whether and to what extent surface recombination is limiting the PL of hex-SiGe alloys. For this purpose, temperature dependent photoluminescence measurements were performed on nanowires with and without effectively proven surface passivation schemes. Case studies were performed for passivation schemes that were earlier successfully studied on planar cub-Ge substrates: aluminum oxide (Al_2O_3)[8], a stack of amorphous silicon and aluminum oxide (a-Si:H/Al_2O_3)[9], and a stack of phosphorous oxide and aluminum oxide (PO_x/Al_2O_3)[10]. These passivation schemes were selected as they have demonstrated effective passivation of cub-Ge surfaces with very low effective surface recombination velocities between $S_{\mathrm{eff}} \approx 300$ cm/s and $S_{\mathrm{eff}} \approx 2.7$ cm s^{-1} [8–10].

2. RESULTS

The hexagonal GaAs/SiGe core/shell nanowires studied in this work were grown using an identical fabrication method as described by Fadaly *et al.*[7]. An overview of the nanowire sample characteristics can be found in Table 1. For the nanowires, several proven passivation films were investigated including a 22 nm thick film of Al_2O_3, a stack of 2 nm a-Si:H capped with 11 nm Al_2O_3 (a-Si:H/Al_2O_3), and a stack of 4 nm PO_x capped with 10 nm Al_2O_3. Details about the process details of these passivation schemes can be found in the work of Berghuis *et al.*[8], Berghuis *et al.*[9], and Theeuwes *et al.*[10], respectively.

Information about (surface-related) non-radiative recombination of the nanowires was obtained via time resolved PL and temperature dependent PL. For the latter, the integrated PL (normalized at a low temperature, typically 4 K) was measured as function of inverse temperature. In this way, the normalized PL represents the internal quantum efficiency or photoluminescence efficiency (η_{PL}) of the nanowires. This quantity relates in a quantitative way to both radiative and non-radiative recombination processes:

$$\eta_{PL} = \frac{R_{rad}}{R_{rad} + \sum_i R_{non-rad,i}} = \frac{1}{1 + \sum_i \frac{\tau_{rad}}{\tau_{non-rad,i(T)}}}. \quad 1$$

The thermal activation energy of the non-radiative recombination mechanisms can typically be described by the Arrhenius relation for thermal activation[11,12]. The temperature dependence of the internal quantum efficiency has consequently the form of[11–13]:

$$\eta_{PL}(T) = \frac{1}{1 + \sum_i \frac{\tau_{rad}}{\tau^{(0)}_{nonrad,i}} exp\left(\frac{E_{a,i}}{k_B T}\right)} = \frac{1}{1 + \sum_i C_i exp\left(\frac{E_{a,i}}{k_B T}\right)}, \quad 2$$

with $E_{a,i}$ the activation energy of the ith non-radiative recombination process and C_i the ratio of the radiative and non-radiative lifetime of the process. This quantity is also referred to as the quenching rate of the ith non-radiative recombination process. Both the radiative lifetime and C_i are expected to be independent of temperature[14]. The quenching rates represent the strength of the non-radiative recombination and can be used to quantify potential reductions in non-radiative (surface) recombination as a consequence of surface passivation. For the PL measurements, substrates with nanowire arrays (typical pitch ~2 µm) were mounted in a helium-flow cryostat. A 976 nm laser with a spotsize of ~40 µm was employed to excite the wires. The PL signal was spectrally resolved using a Fourier Transform Infrared Spectroscopy (FTIR) setup that contains both a HgCdTe detector (used for hex-Ge samples in this work) and InGaAs detector (used for hex-SiGe samples in this work). The signal contribution from the laser and cub-Ge were filtered out using a cub-Ge long-pass filter.

For the TRPL measurements, individual SiGe wires were mechanically placed onto a gold coated silicon wafer. A SiO_2 layer was deposited on top of the gold to prevent direct contact between the wires and the gold. The individual wires were excited with a femtosecond pulsed laser operating at a wavelength of 1030 nm with a pulse frequency of 40 MHz, pulse width of 100 fs, and spotsize of ~3 µm. A superconducting nanowire single-photon detector (SNSPD) from the brand Single Quantum was used to measure the PL signal as a function of time. The reflection from the laser was filtered out using a 1350 nm long pass filter. The lifetime is extracted from the time resolved PL measurements by a fitting the PL decay as a function of time with a mono exponential decay.

Sample name	Nanowire compositio n	Diameter (µm)	Length (µm)	Aspec t ratio	Passivation scheme	Surface treatment	T_{PDA} (°C)	S_{eff} on cub-Ge (cm s^{-1})
H05916	$Si_{0.23}Ge_{0.77}$	0.43 ± 0.07	1.6 ± 0.4	~3.7	Al_2O_3 (22 nm)	1% $HF_{(aq)}$	425	~300 [8]

H06801	Ge	1.7 ± 0.6	2.9 ± 0.5	~1.7	a-Si:H/Al_2O_3 (2/11nm)	20% $HBr_{(aq)}$	325	~2.7 [9]
H06950	$Si_{0.23}Ge_{0.77}$	0.617 ± 0.02	5.62 ± 0.02	~9.1	PO_x/Al_2O_3 (4/10nm)	none	250	~8.9 [10]

Table 1 Overview of nanowire samples discussed in this work. Both the nanowire characteristic as the passivation schemes applied to them are listed. The abbreviation T_{PDA} stands for anneal temperature. The last column shows S_{eff} measured on planar cubic germanium wafers.

Fig. 1a-c demonstrate that excellent conformality of plasma-enhanced ALD Al_2O_3 can be obtained on hex-SiGe nanowires. The figure shows a TEM image of a single hexagonal SiGe nanowire with aspect ratio ~27 after it has been subjected to 200 cycles of the plasma enhanced ALD Al_2O_3 process. The wire, originating from a nanowire array with pitch ~2 µm, shows along its complete length an equally thick Al_2O_3 film (Fig. 1a–c). As expected, the ALD process allows thus for good conformality on these nanostructures. The film measures about 22 nm, which is what one expects based on the GPC of this process (GPC ≈ 1.1 Å/cycle) [15].

The influence of the Al_2O_3 film on the integrated photoluminescence of the hex-$Si_{0.23}Ge_{0.77}$ nanowires is shown in Fig. 1d. This figure shows the integrated PL as a function of inverse temperature for SiGe NWs with and without Al_2O_3 passivation film. The PL intensities of the as-grown wires (black) and the passivated wires (red) have been normalized at 4 K. The latter implies that the vertical axis also represents the internal quantum efficiency. As expected, the internal quantum efficiency decreases with temperature due to the activation of non-radiative recombination mechanisms. For both the passivated and unpassivated wires, the quenching of the PL with temperature seems to be characterized by two knees. This implies that two separate non-radiative recombination channels. Consequently, the data is fitted with Arrhenius equation using two terms, yielding activation energies of $E_{a,1} \approx 3.5$ meV and $E_{a,2} \approx 26$ meV. The fits are represented by solid lines in Fig. 1d. When comparing the passivated and as-grown wires, it seems that the PL of the Al_2O_3 passivated wires first slightly decreases and subsequently increases with increasing temperature. This is also reflected by the slightly lower quenching rate for the passivated wires ($C_{2,pass} \approx 100$ a.u. vs $C_{2,unpass} \approx 183$ a.u.) obtained by the Arrhenius fit, and the 66% higher absolute PL intensity at the highest measurable temperature (90 K). If the non-radiative recombination can be (partially) attributed to the surface, this means a slight reduction of the surface recombination.

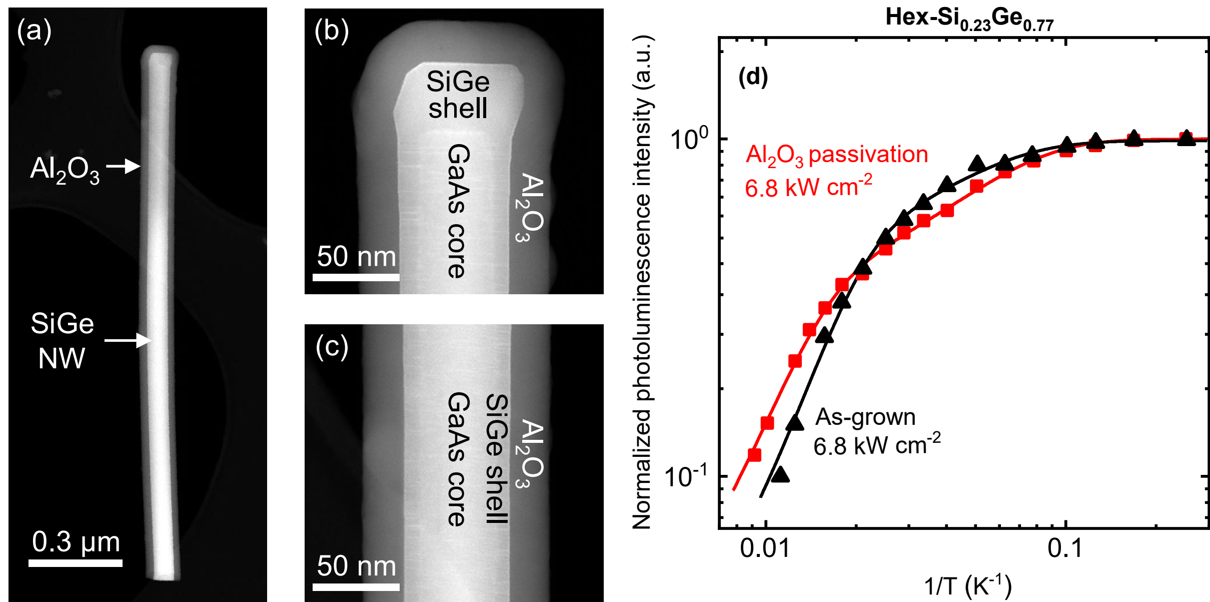

Fig. 1 (a) High-Angle Annular Dark-Field Scanning Transmission Electron Microscopy (HAADF-STEM) image of a hexagonal SiGe nanowire (length ≈ 1.7 µm, diameter ≈ 60 nm, AR ≈ 27, pitch ≈ 2 µm) coated with approximately 22 nm PEALD Al_2O_3. (b) A close-up of the top part of the nanowire. (c) A close-up of the lowest part of the nanowire. (d) Arrhenius representation of the photoluminescence intensity as function of inverse temperature for hex-$Si_{0.23}Ge_{0.77}$ nanowires without and with Al_2O_3 passivation film. The integrated PL intensities are obtained for an excitation density of 6.8 kW/cm^2 and normalized to their respective intensity at 4 K. The data is fitted with the Arrhenius equation (solid lines through the data).

Fig. 2a-d show TEM images of a single hexagonal SiGe nanowire after it has been subjected to 40 seconds PECVD a-Si:H and subsequently 100 cycles of plasma enhanced ALD Al_2O_3. The properties of the nanowire are identical to those described in Fig. 1a-c. The Al_2O_3 capping layer is along the whole length of the nanowire the same thickness of 10.5±0.5 nm, which indicates a very conformal coating. The PECVD a-Si:H interlayer is present along the whole nanowire as well, which is important. When considering the film thickness, it is observed that the a-Si:H is substantially thicker on the top (3.0±0.5 nm) than on the side walls (1.5±0.5 nm). The lower thickness on the sides of the nanowire is likely related to a lower flux of reactive plasma species. For PECVD, the latter is an important factor for the growth rate, this in contrast to ALD. The lower thickness on the sidewalls is not considered problematic and becomes only undesired when the a-Si:H gets completely oxidized by the subsequent PEALD Al_2O_3 process.

The effect of the a-Si:H/Al_2O_3 stacks on the integrated photoluminescence of the hex-Ge nanowires is shown in Fig. 2e. The PL intensities of the as-grown wires (black) and the passivated wires (red) have been normalized at 6 K. The PL quenching with temperature seems to be characterized by two knees for both the passivated and unpassivated wires, similar as in Fig. 1e. The Arrhenius fits of the data (solid lines), yield similar activation energies of $E_{a,1} \approx 4.4$ meV and $E_{a,2} \approx 26$ meV. When comparing the passivated and as-grown wires, it becomes evident that they show very similar behavior. The PL of the passivated wires decrease a little bit less with temperature ($C_{2,pass} \approx 29$ a.u. vs $C_{2,unpass} \approx 55$ a.u.) and the absolute PL intensity is about 30% higher at room temperature. The latter hints for a slight reduction in non-radiative recombination pathways, presumably related to the surface.

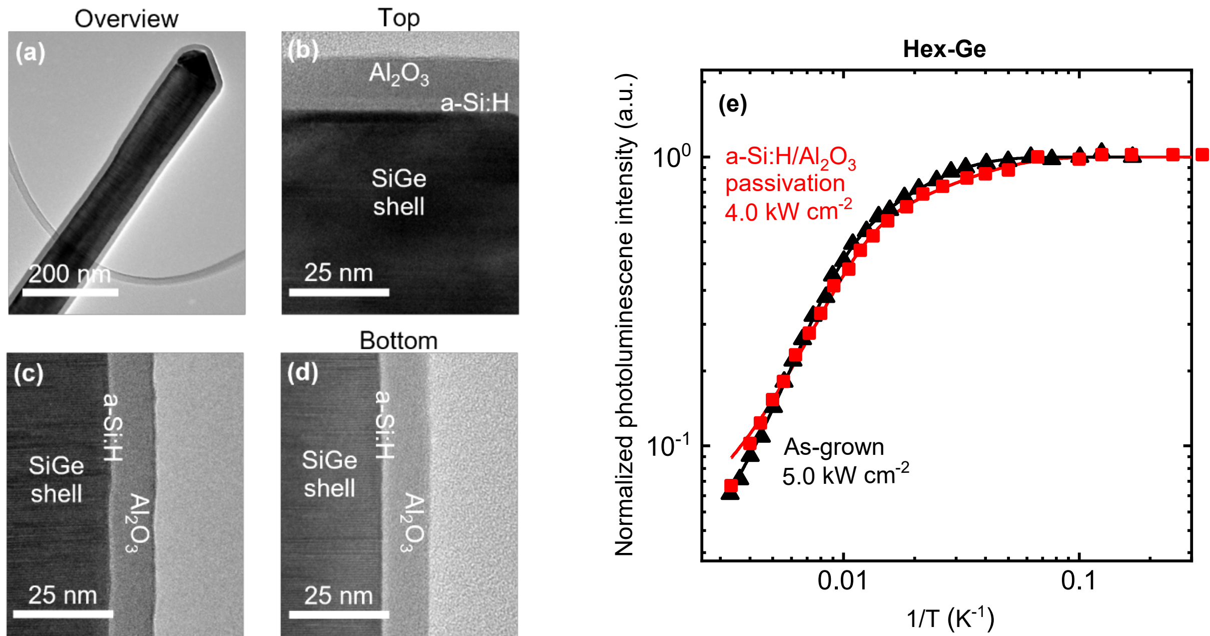

Fig. 2 (a) Bright-Field Scanning Transmission Electron Microscopy (BFTEM) image of the upper half of a hexagonal GaAs/SiGe core/shell nanowire (length ≈ 1.7 μm, diameter ≈ 60 nm, AR ≈ 27, pitch ≈ 2 μm) coated with the a-Si:H/Al_2O_3 stack. (b) A close-up of the top part of the nanowire. The a-Si:H interlayer is approximately 3.0±0.5 nm thick, while the Al_2O_3 capping is 10.5±0.5 nm nm. (c) close-up of the middle part of the nanowire (~1 μm from the top). (d) close-up of the lowest part of the nanowire (~2 μm from the top). The a-Si:H interlayer measures 1.5±0.5 nm and the Al_2O_3 capping 10.5±0.5 nm. (e) Arrhenius representation of the photoluminescence intensity as function of inverse temperature for hex-Ge nanowires with and without a-Si:H/Al_2O_3 passivation stack. The integrated PL intensities are normalized to their respective intensity at 6 K. The data is fitted with the Arrhenius equation (solid lines through the data). Excitation densities of 4 and 5 kW/cm^2 are used for the passivated and as-grown wires respectively.

The conformality of the PO_x/Al_2O_3 deposition process used in this work has already been demonstrated on nanowires in earlier work by Black *et al.*[16] and Theeuwes *et al.*[17]. For this stack we therefore focus only on the changes in photoluminescence as a consequence of applying this stack on the surface of hex-SiGe nanowires. Figure 3 shows the integrated PL intensity as function of inverse temperature for hex-$Si_{0.12}Ge_{0.88}$ nanowires without (black) and with a PO_x/Al_2O_3 passivation stack (red). The PL intensities are normalized with respect to their intensities at 4 K. The temperature behavior of the integrated PL can be described by the Arrhenius equation using three terms, as observed before for this generation of hex-SiGe nanowires[7]. Due to the limited range of the wires without passivation, a fair comparison of the fit parameters with the passivated wires seems questionable. From the Fig. 3 it is however clear that the PL of the wires without the stack decrease substantially less with increasing temperature. Additionally, the absolute integrated PL at 160 K (the highest measurable temperature) is 40% lower after applying the passivation film. These observations indicate no reduction in surface recombination by the PO_x/Al_2O_3 stack.

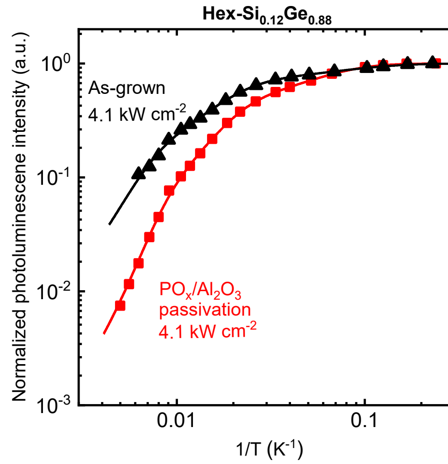

Fig. 3 Arrhenius representation of the photoluminescence intensity as function of inverse temperature for hex-$Si_{0.12}Ge_{0.88}$ nanowires without and with a PO_x/Al_2O_3 passivation stack. The integrated PL intensities are obtained for an excitation density of 4.1 kW/cm^2 and normalized to their respective intensity at 4 K. The data is fitted with the Arrhenius equation (solid lines through the data).

In Fig. 4 the integrated photoluminescence of various passivated hex-Ge and hex-SiGe nanowires is presented with respect to the same nanowires without the passivation film (dashed line). The data is collected at room temperature (293 K) at relatively high excitation densities (4.0 - 7.4 kW cm^{-2}). The overview includes also nanowires discussed in the previous sections. Fig. 4 shows that in most cases the passivation film slightly enhances the PL except for the thermal ALD Al_2O_3 film and the PO_x/Al_2O_3 stack. Secondly, and more generally, the presented passivation schemes show all a relatively mild impact on the integrated photoluminescence of the nanowires, i.e., the deviation from the nanowires without the passivation schemes (dashed line) is mostly within a factor of two. The latter indicates a relatively small influence of the surface on the photoluminescence.

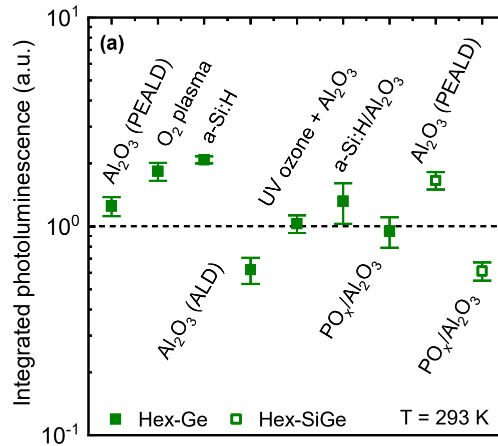

Fig. 4 Overview of the integrated photoluminescence of various hex-Ge (closed symbols) and hex-SiGe (open symbols) nanowires passivated with various passivation schemes. The integrated PL is normalized with respect to the integrated photoluminescence of the same nanowires without the passivation scheme. The nanowires are measured 293 K with the exception for the SiGe nanowires with the Al_2O_3 and PO_x/AlO_x passivation for which the highest measurable temperatures were 90 K and 160 K respectively. Excitation densities used for the measurement vary slightly per sample but lie between 4.0 and 7.4 kW cm^{-2}.

When considering the nanowires that were studied in more detail (Fig. 1 – Fig. 3), we observe that despite some improvements by the Al_2O_3 and a-Si:H/Al_2O_3 passivation schemes, the decrease of the PL with temperature is still very similar (between one and two orders of magnitude). The latter indicates that the

non-radiative recombination channels are still very active after applying the passivation films. This could either mean that passivation is not very effective or that the surface is not the main cause for non-radiative losses in these nanowires. Considering that these passivation schemes have demonstrated very low surface recombination velocities on cubic germanium and cubic silicon, the former seems unlikely. Moreover, the quick screening of several other passivation schemes (Fig. 4) shows that all tested films and pre-treatments have only mild impact on the PL, which also hints for a small influence of the surface on the PL rather than a strongly limiting surface. These two reasons make it most likely that the surface is not one of the main non-radiative recombination channels in these nanowires.

3. CONCLUSION

In conclusion, several passivation schemes that have demonstrated low surface recombination velocities on cubic germanium have been applied to hex-Ge and hex-SiGe nanowires. At room temperature and relatively high excitation densities (4 - 7.5 kW cm^{-2}), these passivation schemes only lead to relatively small changes in the integrated photoluminescence compared to the nanowires with a native surface. Considering these observations, we conclude that the hex-(Si)Ge surface is most likely not strongly influencing, hence not limiting, the PL in the high excitation regime ($S_{eff,max} < 3.9 \times 10^4$ cm s^{-1}). The decrease in internal quantum efficiency with increasing temperature may therefore stem predominantly from non-radiative recombination in the bulk of the hex-(Si)Ge. For hex-SiGe based devices with micrometer dimensions operating at relatively high excitation densities, like nano-laser, the results of this research imply that surface recombination will most likely not be a bottleneck.

References

1. D. A. B. Miller: Device Requirement for Optical Interconnects to Silicon Chips., in Proc. of IEEE Special Issue on Silicon Photonics (2009), pp. 1166–1185.
2. V. Reboud, A. Gassenq, J. M. Hartmann, J. Widiez, L. Virot, J. Aubin, K. Guilloy, S. Tardif, J. M. Fédéli, N. Pauc, A. Chelnokov, and V. Calvo: Progress in Crystal Growth and Characterization of Materials Germanium based photonic components toward a full silicon / germanium photonic platform. *Progress in Crystal Growth and Characterization of Materials* **63**, 1–24 (2017).
3. D. A. B. Miller: Device Requirements for Optical Interconnects to Silicon Chips. *Proceedings of the IEEE* **97**, 1166–1185 (2009).
4. L. C. Kimerling and J. Michel: Monolithic Microphotonic Integration on the Silicon Platform. *ECS Transactions* **41**, 3–13 (2011).
5. K. Zinoviev, L. G. Carrascosa, J. S. del Rio, B. Sepúlveda, C. Domínguez, and L. M. Lechuga: Silicon Photonic Biosensors for Lab-on-a-Chip Applications. *Advances in Optical Technologies* 383927 (2008).
6. J. D. Joannopoulos and M. L. Cohen: Electronic properties of complex crystalline and amorphous phases of Ge and Si. I. Density of states and band structures. *Physical Review B* **7**, 2644–2657 (1973).
7. E. M. T. Fadaly, A. Dijkstra, J. R. Suckert, D. Ziss, M. A. J. Van Tilburg, C. Mao, Y. Ren, V. T. Van Lange, K. Korzun, S. Kölling, M. A. Verheijen, D. Busse, C. Rödl, J. Furthmüller, F. Bechstedt, J. Stangl, J. J. Finley, S. Botti, J. E. M. Haverkort, and E. P. A. M. Bakkers: Direct-bandgap emission from hexagonal Ge and SiGe alloys. *Nature* **580**, 205–209 (2020).
8. W. J. H. Berghuis, J. Melskens, R. J. Theeuwes, B. Macco, M. A. Verheijen, and W. M. M. Kessels: Surface Passivation of Germanium by Atomic Layer Deposited Al2O3 Nanolayers. *Journal of materials research* **36**, 571–581 (2021).
9. W. J. H. Berghuis, J. Melskens, B. Macco, R. J. Theeuwes, L. E. Black, M. A. Verheijen, and W. M. M. (Erwin) Kessels: Excellent surface passivation of germanium by a-Si:H/Al_2O_3 stacks. *Journal of Applied Physics* **130**, 135303 (2021).

10. R. J. Theeuwes, W. J. H. Berghuis, B. Macco, and W. M. M. Kessels: Excellent Passivation of Germanium Surfaces by PO_x/Al_2O_3 stacks. *xxx* **xxx**, xxxxxxx (n.d.).
11. J. D. Lambkin, L. Considine, S. Walsh, G. M. O. Connor, C. J. Mcdonagh, and T. J. Glynn: Temperature dependence of the photoluminescence intensity of ordered and disordered In0.48Ga0.52P. *Appl.Phys.Lett.* **65**, 73–75 (1994).
12. M. A. Reshchikov: Temperature dependence of defect-related photoluminescence in III-V and II-VI semiconductors. *Journal of Applied Physics* **115**, 012010-1–15 (2014).
13. M. A. Reshchikov: Mechanisms of Thermal Quenching of Defect-Related Luminescence in Semiconductors. *Physica Scripta* **218**, 2000101 (2021).
14. A. Dijkstra: Doctoral Dissertation: Optical Properties of Direct Band Gap Group IV Semiconductors, Eindhoven University of Technology, 2021.
15. G. Dingemans and W. M. M. Kessels: Status and prospects of Al_2O_3-based surface passivation schemes for silicon solar cells. *Journal of Vacuum Science & Technology A* **30**, 1–24 (2012).
16. L. E. Black, A. Cavalli, M. A. Verheijen, J. E. M. Haverkort, E. P. A. M. Bakkers, and W. M. M. Kessels: Effective Surface Passivation of InP Nanowires by Atomic-Layer-Deposited Al2O3 with POx Interlayer. (2017).
17. R. J. Theeuwes, J. Melskens, W. Beyer, U. Breuer, L. E. Black, W. J. H. Berghuis, B. Macco, and W. M. M. Kessels1: POx/Al2O3 stacks for surface passivation of Si and InP. *Sol. Energy Mater. Sol. Cells* **246**, 111911 (2022).

4. INTRODUCTION: CONTACT FORMATION AND ELECTRICAL CHARACTERIZATION

This part summarizes all activities towards ohmic contact formation and electrical characterization on hexagonal $Si_{20}Ge_{80}$ nanowires, which typically have a n-type non-intentional doping concentration in the mid $10^{18}cm^3$. We start with simple metal-semiconductor contacts and explore annealing strategies to form metal-alloy-semiconductor junctions. To further reduce the barrier height for transparent, ohmic contacts two semiconductor doping schemes were studied. Doping via solid state diffusion from a phosphorus doped oxide, as well as ion implantation. Electrical characterizations are reported using 2-point and 4-point measurements on the processed nanowires.

5. METAL CONTACTS

Simple metal-semiconductor junctions were fabricated using evaporated Ti, Ni, and Al as contacts which were typically covered with an additional Au layer. The lithographically defined contact openings on the nanowires were exposed to a short BHF etch, rinsed, dried, and immediately loaded into the evaporator to promote a clean, oxide-free interface.

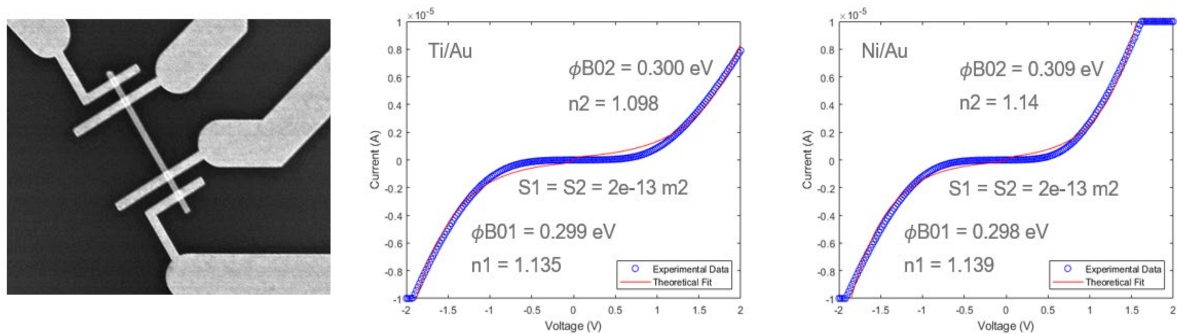

Figure 1 Properties of metal contacts to HexSiGe NWs. Independent of contact metal (Ti, Ni, Al) devices show large Schottky barriers.

The electrical results (Figure 1) show the signatures of a double sided Schottky contact, independent of metal and different metal work function used. This indicates that the barrier is too wide and that defects at the metal-semiconductor interface pin the fermi level. From fitting of the I-V curves, a barrier height of 300meV was obtained for all metal contacts used.

6. POST ANNEALING OF METAL CONTACTS

It is well documented, that metal-semiconductor Schottky barriers can be lowered by the formation of an intermetallic compound or alloy. We explored to systems, Ni-SiGe and Al-SiGe. Starting with the first system, inter-diffusion, and reactions of the Ni-SiGe couple can form silicide and germanide compounds interfacing with the semiconductor. Controlling the Nickel process proved to be difficult (Figure 2) and resulted in a large spread of the contact properties when annealed at 290°C. Increasing the annealing to 300°C resulted in low yields due to loss of contact. Nevertheless a high contact resistivity could be obtained in one working TLM device in the order of 3.5x 10^{-3} Ohmcm. Therefore, work with Ni-alloying using unintentionally doped wires was discontinued.

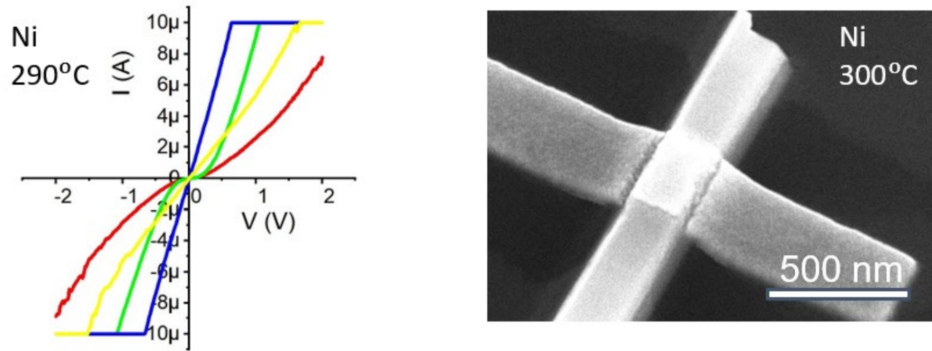

Figure 2 Thermal annealing of Ni-SiGe contacts. Some contacts turn from Schottky to ohmic. Process control is critical and too high temperature or reaction time can lead to loss of contact as illustrated by the formation of a gap at the Ni-nanowire interface.

The Al-SiGe system differentiates significantly from the Ni-SiGe as SiGe is soluble in Al, and furthermore Al is a p-dopant in group IV semiconductors. Figure 3 shows results of annealing Al/Hex-SiGe contacts at 400°C, 10s and illustrates the significant material diffusion during the process.

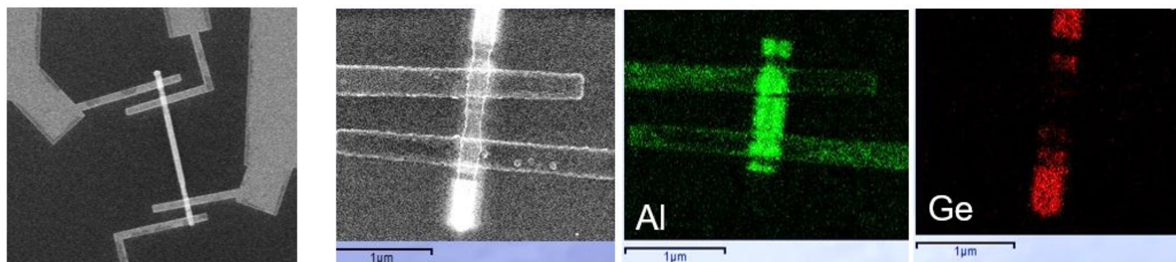

Figure 3 Diffusion during aluminum contact annealing at 400C 10sec. SEM images reveals a modified morphology close to the contacts, while EDS shows extensive diffusion of Al into the nanowire and corresponding out-diffusion of SiGe into the contact leads.

Si and Ge are soluble in Al and fast diffusors. The SiGe is thus dissolved from the nanowires and transported into the Al leads, while the aluminum travels the reverse direction into the nanowire. This can be well observed in the EDS images in Figure 3. The process is so efficient that large segments of the nanowire become fully metallic (Al) and even leading to a shortening of nearby contacts. By exploring lower annealing temperatures and keeping the time constant, an optimized process condition was

achieved (Figure 4). At 310°C, all contacts showed ohmic behavior and EDS measurements showed a very limited aluminum diffusion.

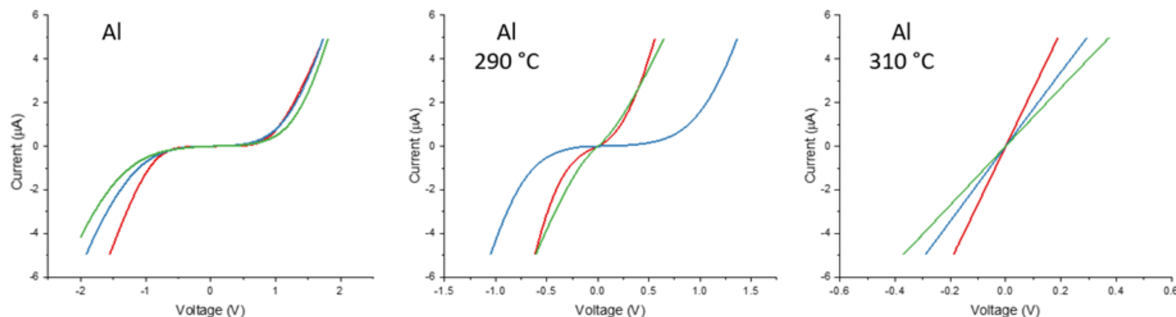

Figure 4 Effect of Al contact annealing temperature on electrical properties of Hex-SiGe nanowires. Above 310°C, the contacts turn ohmic, and show high uniformity.

The samples with ohmic contacts show an increase in resistance with increasing distance between the contacts. A careful TLM study to determine the resistivities and contact resistance is in progress. Annealed Al contacts is thus the preferred method to contact as grown Hex-SiGe nanowires.

7. DOPING

Doping processes often involve elevated temperatures. This can be high-temperature drive-in step of an impurity, or a high-temperature step to recover crystal lattice defects, or to achieve a high activation of the impurity in the lattice. Thus, the available temperature budget is critical to access. Working with core-shell nanowires from III-V and group IV materials is a significant challenge, as thermal properties are very different and intermixing and chemical reactions must be avoided. A beneficial situation would be to first remove the GaAs core, and subsequently perform the high-temperature processes. Therefore, the selective etching of the GaAs core was investigated. Considering that the SiGe shell is about 60nm thick, while the nanowires are about 6 µm long, the required selectivity between GaAs and SiGe must be > 100. Moreover, the diffusion of the bromine-methanol solution is expected to slow down over time as the core is etched out, increasing the need for high selectivity.

An effective etchant for many III-V semiconductors which does not contain hydrogen peroxide is the bromine-methanol solution. At low bromine concentration of 1%, this solution is also selective over SiGe. Figure 5 shows etching results obtained with a 1% solution at room temperature. EDS clearly shows the successful removal of the GaAs core. Overall, this approach allows to prepare GaAs-free Hex-SiGe samples that are robust at high temperatures for solid state doping.

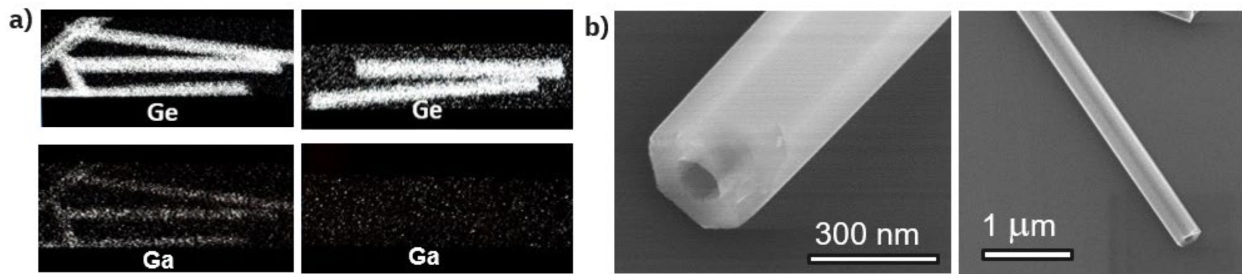

Figure 5 Selective etching of 3um long GaAs core from $Si_{20}Ge_{80}$ nanowires using 1% bromine-methanol solution. a) EDS of nanowires before and after wet etching. b) SEM images of nanowires with etched-out core.

8. DOPING BY SOLID STATE DIFFUSION

Solid state diffusion of impurities is conceptually a simple method and widely used for doping of planar devices. A typical impurity source are highly doped (P,B, Zn..) glass films. Here 20nmm thick phosphorus doped SiOx layers were used, deposited by PECVD (150 SCCM SiH_4, 700 SCCM N_2O and 50 SCCM of PH_3) with an undoped SiOx capping layer. The aim of the solid-state diffusion is to heavily dope the contacts areas, or alternatively the entire device. In the examples shown in Figure 6, the nanowires were entirely covered with the doped oxide, and afterwards annealed at 600C, 5min and 800C 30sec. After annealing the oxide was partially removed and Ni contacts were deposited.

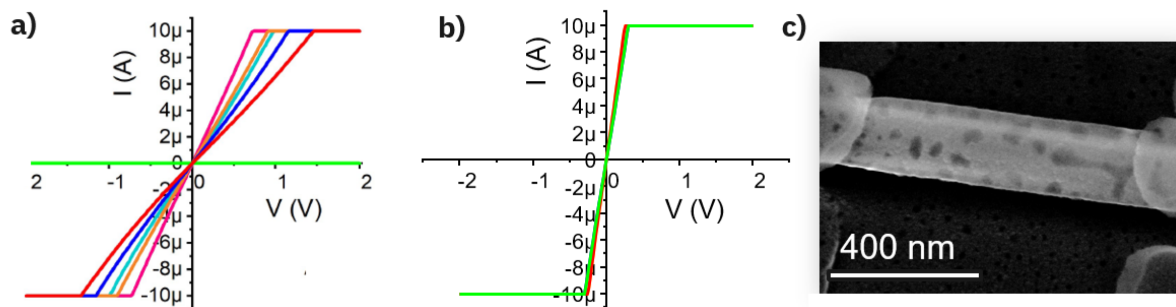

Figure 6 Doping of Hex-SiGe nanowire by thermal diffusion form a solid phosphorus source. a) I-V after 600C 300sec diffusion, b) I-V after 800C 30sec diffusion, c) nanowire after 800C diffusion showing defects.

The electrical measurements shows that the 600C annealed sample exhibits nearly linear, ohmic behavior, while the 800C sample has perfectly linear contacts. While this these initial results are very promising, a degradation of the nanowire was clearly observed in both cases. We note that while the concept appears simple, the actual implementation was not as straightforward. More work is needed to optimize the processes and to confirm the first n-type contact results with the most recent Hex-SiGe samples from TU/e which have a lower (As) non-intentional impurity concentration.

9. DOPING BY IMPLANTATION

Doping by ion implantation is the standard method in Si technology, due to its broad versatility and reproducibility. Typically mostly used in planar technology, its applicability was also demonstrated for 3D structures such as fins and nanowires. The constrains for non-planar samples is to guarantee a sufficiently large interface between the defect-free crystal and the implanted and amorphized structure. This allows the formation of a well behaved recrystallisation front during defect annealing. A unique challenge in addition is to verify that our metastable material crystallizes indeed into the hexagonal phase and does not fall back into the thermodynamic more stable cubic lattice. A set of chips with nanowires were As

implanted at 18kV, $3x10^{14}$ ions/cm^2 which should result in an layer with a charge carrier density of appx. $5x10^{20}$ cm^3. The results are displayed in Figure 7.

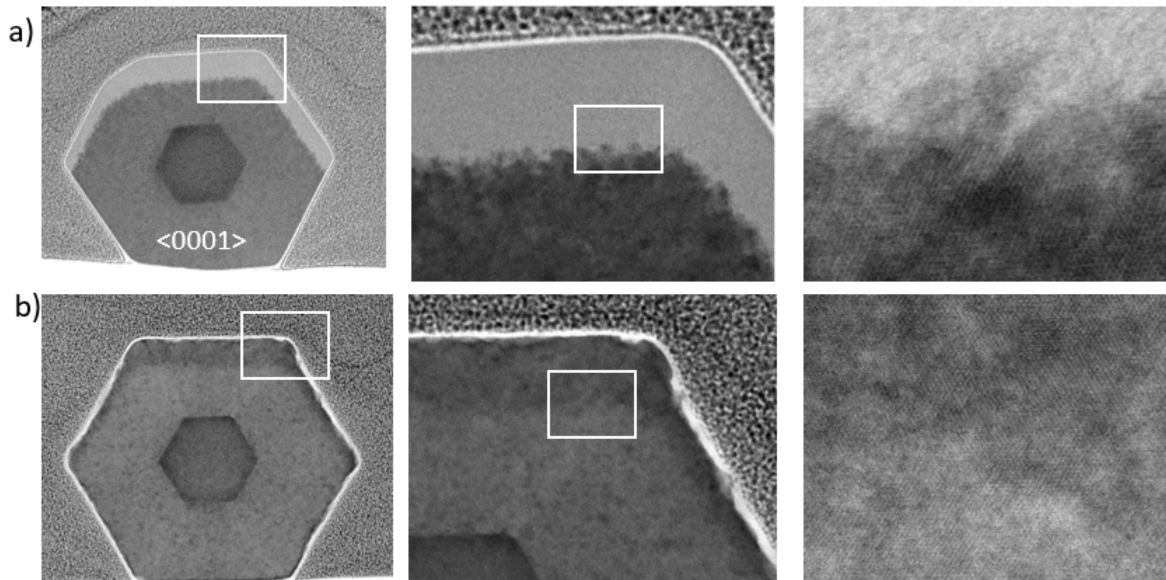

Figure 7 STEM images of an **As** implanted and recrystallized Hex-SiGe nanowire with a WZ GaAs core. a) 18kV As implantation from the top, leading to an amorphized layer, while the lower part remains defect-free. b) After 600C recrystallisation, the image contrast has much reduced, indicating recovery of the lattice, as revealed in rightmost image.

A similar structural result was obtained using 30kV Ga implantation and 600C post anneal, as shown in Figure 8. Here the sample is cut along the (1-100) growth direction, that allows to verify the recovery of the hexagonal phase.

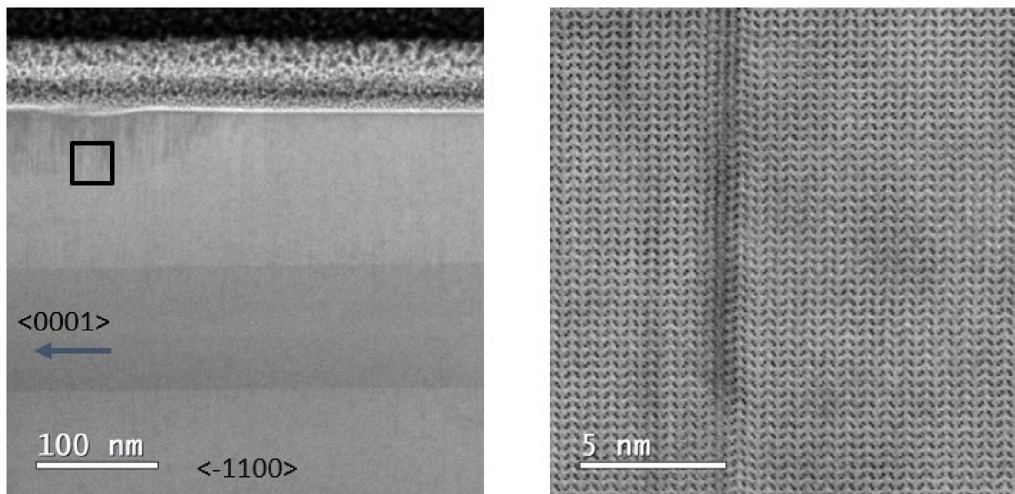

Figure 8 STEM images of an 30kV Ga implanted and recrystallized Hex-SiGe nanowire with a WZ GaAs core cut along the <0001> axis. The high-resolution image indicates recovery of the lattice, with the hexagonal stacking sequence nicely visible.

The n and p doped nanowires were subsequently electrically contacted. A 2-point measurement on the Ga (p-type) nanowire using Al resulted in direct ohmic contacts without the need for annealing. This clearly indicated a successful thinning of the barrier due to the high charge density at the interface. The 2-point resistance was between 2-3kOhm. The collection of a complete TLM dataset is ongoing.

In first experiments, the As (n-type) doped nanowires were contacted with Ni and Al. In both cases, only Schottky contacts were obtained. Therefore, the sample underwent a post-anneal step, as previously described. Here, annealing up to 280°C still showed rectifying behavior, while higher annealing led to a loss of contact. Thus, the highly As doped nanowires showed very similar behavior as the non-intentionally, as grown wires, which are assumed to be n-type doped to appx $3x10^{18}$ cm^{3}. This agrees with observations on cubic Ge, where Fermi-level pinning close to the valence band makes ohmic contact formation very challenging. Nevertheless, it is surprising that the added impurities did not reduce the barrier height significantly. Clearly, these initial experiments need to be repeated before a solid conclusion can be offered.

10. CONCLUSION

We have evaluated various electrical contacting schemes for non-intentionally doped Hex-SiGe nanowires. Simple metal contacts (Ti, Ni, Al) show strong Schottky-type rectifying behaviour with barrier heights around 300mV. Thermal annealing of Ni and Al metal-semiconductor junctions can significantly lower the barrier height and even result in ohmic contact formation. The formation of germanide/silicide interfaces with Ni or an alloyed Al interface are sensitive functions of the annealing conditions. Too high temperatures lead to significant material diffusion processes, with can cause complete loss of contact or metallic shorts between nearby contacts. Process control is particularly important due to the 3D geometry of the nanowire and the typically limited thickness of the metal reservoir. The Ni process shows to be more difficult to control and to reproduce compared with the Al process. The Al-SiGe exchange process results in in-diffusion of Al and formation of an Al-SiGe interface with good electrical transparency.

To improve carrier injection, solid state diffusion doping on Hex-SiGe nanowires was demonstrated. Due to the high temperature needed for efficient diffusion, a selective etch process to remove the GaAs core was developed. Initial 2-point measurements showed ohmic contacts the phosphorus (n-type) Hex-SiGe nanowire. Additional work to reproduce the results is pending.

Finally doping by implantation was performed using As and Ga. The implanted crystals could be recrystallized, and STEM confirmed the recovery of the original lattice. Very promising results obtained with p-type contacts, while reproducing the n-type work will be the ongoing focus in the next months.